Journal of Environmental Chemical Engineering 9 (2021) 105782

Contents lists available at ScienceDirect

Journal of Environmental Chemical Engineering

journal homepage: www.elsevier.com/locate/jece

Optimization of carbamazepine photodegradation on defective TiO_2-based magnetic photocatalyst

Szymon Dudziak [a,*], Zuzanna Bielan [b], Paweł Kubica [c], Anna Zielińska-Jurek [a,*]

[a] Department of Process Engineering and Chemical Technology, Gdansk University of Technology, G. Narutowicza 11/12, Gdańsk 80-233, Poland
[b] Centre for Plasma and Laser Engineering, The Szewalski Institute of Fluid-Flow Machinery, Polish Academy of Science, Fiszera 14, 80–231 Gdańsk, Poland
[c] Department of Analytical Chemistry, Gdansk University of Technology, G. Narutowicza 11/12, Gdańsk 80-233, Poland

ARTICLE INFO

Editor: Dr. Zhang Xiwang

Keywords:
Photocatalysis
Carbamazepine
Process optimization
Magnetic photocatalyst
Factor interactions
Regression model

ABSTRACT

In this work, carbamazepine (CBZ) degradation over defective Fe_3O_4@SiO_2/d-TiO_2/Pt photocatalyst was studied. Within the titania structure, Ti vacancies and Pt nanoparticles were introduced to enhance the photocatalyst's light absorption and influence charge carriers' mobility. For the carbamazepine degradation, process parameters, e.g., temperature, flux intensity, photocatalyst loading, aeration, pH, and addition of H_2O_2, were optimized for 4 or 5 different levels, with the quadratic model including 2-factor interactions determined to analyze the effect of these parameters. Carbamazepine presence and by-product formation were monitored using the HPLC-DAD system together with additional HPLC-TOFMS analysis for further identification of created compounds. Acridine was selected as an additional factor, indicating differences in the performed process of photolysis and photocatalytic CBZ degradation. Pure TiO_2 exhibited the highest efficiency of CBZ degradation under alkaline conditions, while the performed optimization shows that a combination of H^+ and H_2O_2 addition is crucial to achieve high CBZ removal and its mineralization in the presence of Fe_3O_4@SiO_2/d-TiO_2/Pt photocatalyst. The obtained results were discussed concerning photocatalyst structure, generation of reactive oxygen species inside H^+/H_2O_2/photocatalyst system, and the possible effect of introduced Ti vacancies. In terms of reusability, the performance of Fe_3O_4@SiO_2/d-TiO_2/Pt photocatalyst was stable after 8 subsequent cycles of carbamazepine degradation.

1. Introduction

Carbamazepine (CBZ) is often used as an anticonvulsant drug, which has gained considerable attention since its presence was reported in surface waters worldwide [1–4]. Currently, both CBZ and its possible by-products were found to impact the environment negatively [5,6]. Existing reports have shown that carbamazepine is harmful to aquatic organisms at the concentration of 150 mg·dm^{-3} and could bioaccumulate along the trophic chain [7]. Moreover, Wiegman et al. [8] studied the toxicity of acridine, one of the possible by-products of CBZ degradation, to marine algae and found that it was enhanced due to UV light absorption. It is well-known that a similar relationship between the substrate and toxic product can be expected for many of the emerging pollutants [9–11]. Therefore, much attention is recently given to present a complete description of the degradation process and finding the most optimal solution in terms of environmental impact. It results in an ongoing effort to study both efficiency and chemistry of carbamazepine degradation.

Commonly used methods, including biodegradation [12,13], chemical oxidation in the presence of persulfate [14], or chlorine [15], are still far from satisfactory concerning the removal of persistent organic pollutants. Zhou et al. [16] combined UV-induced process with chlorination, getting about 70% of carbamazepine degradation after 60 min. However, toxic chlorinated by-products, such as trichloroacetic acid, dichloroacetonitrile, and trichloronitromethane were formed.

In this regard, the photocatalytic process in which the reactive oxygen species are created in situ remains one of the most promising approaches for water treatment to decompose persistent organic pollutants that are not prone to biological degradation [17,18].

Extensive research is devoted mainly to TiO_2 photocatalytic oxidation. However, to the major challenges of the photocatalytic process belongs the limitations related to the wide band gap of TiO_2, which practically limits the use of solar light in the photodegradation process. Also, unfavorable recombination of photo-excited electrons and holes

* Corresponding authors.
E-mail addresses: dudziakszy@gmail.com (S. Dudziak), annjurek@pg.edu.pl (A. Zielińska-Jurek).

https://doi.org/10.1016/j.jece.2021.105782
Received 30 March 2021; Received in revised form 15 May 2021; Accepted 29 May 2021
Available online 2 June 2021

cause a significant reduction in the photocatalytic reaction's quantum efficiency. Moreover, there are several problems with recovery and cyclic utilization of the powdered nano-TiO_2 particles suspended in the treated water in a technological process.

In this regard, the present study pertains to synthesis and characteristic of Fe_3O_4@SiO_2/d-TiO_2/Pt magnetic photocatalyst, which was applied in the photodegradation process. The functionality of TiO_2 nanosized semiconductor photocatalyst and magnetic compound (spinel ferrite particles of Fe_3O_4) enables easy separation and reuse of nanometric size particles from the treated water after the purification process [19,20]. The SiO_2 interlayer was introduced to prevent charge carriers' transfer from TiO_2 to Fe_3O_4. Furthermore, Pt nanoparticles with plasmonic properties were deposited on the composite surface to enhance photocatalytic activity. At the same time, the Schottky barrier generated due to the significant difference of work function between the semiconductor (TiO_2) and a noble metal (Pt) forms an inner built-in electrical field, which improves the migration of the photogenerated electrons [21]. Additionally, the intrinsic crystal defects present in the structure of TiO_2 (mostly oxygen and titanium vacancies) change the charge carriers' reactivity, extending the light absorption to the visible region [22,23].

The photodegradation process's optimal design targeting non-biodegradable compounds such as carbamazepine to non-toxic and more susceptible to biodegradation intermediates is challenging and has become one of the most important issues in environmental protection and management. Therefore, the as-prepared magnetic nanocomposite was studied in the process of CBZ photodegradation, with six different parameters being considered for optimization: photocatalyst loading, pH, aeration, temperature, irradiation intensity, and H_2O_2 addition, as well as their mutual interactions, varied on 4 or 5 different levels, based on the central composite design (CCD). Furthermore, the photodegradation pathway was studied to gain a better inside into the mechanism of carbamazepine degradation and mineralization.

2. Experimental

2.1. Photocatalyst preparation and characterization

The commercially available Fe_3O_4 particles with a particle size of about 50–60 nm (Alfa Aesar, Kandel, Germany) were used to prepare the composite with magnetic properties. The surface coating was achieved using the previously developed method, based on zeta potential changes [24]. Briefly, magnetite particles were dispersed in w/o microemulsion using cyclohexane as oil phase, isopropanol as co-surfactant, and hexadecyltrimethylammonium bromide (CTAB) as a surfactant. Then tetraethyl orthosilicate hydrolysis and deposition of modified TiO_2 particles proceeded in two subsequent reactions. Before deposition, titanium(IV) oxide particles were prepared from hydrolysis of titanium (IV) butoxide inside the oxidative environment of HIO_3 to enable the creation of Ti vacancies inside its structure. Moreover, the surface of TiO_2 particles was modified by 0.1 mol% of Pt nanoparticles, reduced from hexachloroplatinate acid. The more detailed preparation procedure is presented in the Supporting Materials.

During the optimization procedure, the appropriate amount of the magnetic photocatalyst was synthesized in batches. Each part was individually characterized by the BET method for the specific surface area and X-ray diffractometry (XRD, phase content, and crystallites size) analyses to confirm structural consistency between the series. At the same time, other characterizations were performed for the final mixture.

XRD analysis was performed using the Rigaku MiniFlex 600 X-ray diffractometer (Tokyo, Japan) equipped with a sealed tube X-ray generator (a copper target; operated at 40 kV and 30 mA). Data was collected in the 2θ range of 5–80°. Scan speed and scan steps were fixed at $1^\circ \cdot min^{-1}$ and 0.01°, respectively. The analysis was based on the International Centre for Diffraction Data (ICDD) database.

Nitrogen adsorption isotherms (BET method for the specific surface area) were recorded using the Micromeritics Gemini V (model 2365) (Norcross, GA, USA) instrument at 77 K (liquid nitrogen temperature).

The light-absorption properties were measured using diffuse reflectance (DR) spectroscopy in the range of 200–800 nm, and the data were converted to obtain absorption spectra. The bandgap energy of obtained samples was calculated from $(F(R)\cdot E)^{0.5}$ against E graph, where E is photon energy, and F(R) is Kubelka-Munk function, proportional to the radiation's absorption. The measurements were carried out using ThermoScientific Evolution 220 Spectrophotometer (Waltham, MA, USA) equipped with a PIN-757 integrating sphere. As a reference, $BaSO_4$ and Fe_3O_4@SiO_2/D-TiO_2 were used.

Samples morphology and the formation of the core-shell structure were determined by transmission electron microscopy observations (TEM, FEI Europe, Tencai F20 X-Twin).

The intrinsic defects formation of TiO_2 photocatalysts was confirmed based on electron paramagnetic resonance (EPR) analysis using RADIOPAN SE/X-2547 spectrometer operating at room temperature frequency in range 8.910984–8.917817 GHz.

The electrophoretic mobility of particles at different pH values was investigated using Nano-ZS Zetasizer dynamic light scattering detector (Malvern Instruments, UK) equipped with a 4.0 mW internal laser.

2.2. Measurements of carbamazepine photocatalytic degradation - Design of experiment

Commercial carbamazepine (≥ 98%, Sigma-Aldrich) was used to prepare 14 $mg\cdot dm^{-3}$ CBZ solution. A total number of 79 degradation processes were performed to optimize process conditions using a 50 cm^3 quartz reactor equipped with a stirrer and a cooling jacket connected to a thermostat. Xenon lamp (6271H, Oriel, Germany) was used as a UV-Vis irradiation source. Before each analysis, UV light's intensity at 310–380 nm was measured at the front of the reactor, and its position was adjusted to obtain the desired flux value. Six different factors were considered inside the investigated system – pH, photocatalyst loading, flux intensity, temperature, H_2O_2 addition, and airflow through the reactor, which were varied on 4 or 5 different levels, based on the central composite design (CCD). A deviation from classical CCD resulted from a desire to investigate each variable in possibly board range, together with keeping − 1 levels of aeration and H_2O_2 addition at 0, which ultimately braked the symmetry of star points alignment (a and -a). Despite this, general methodology remained similar, and a summary of varied factors is presented in Table 1. For pH adjustment, a 5 M solution of NaOH was used together with 5% HCl (w/w), and 30% hydrogen peroxide solution (w/w, provided by Chempur, Poland) was used as a source of H_2O_2. A full design matrix, together with coding details, is shown in Section 2 in the Supporting Materials.

Three measurements at the central point (each factor at 0 level) were performed to estimate the experimental error of obtained results. Additionally, a series of dark reaction experiments were carried out for different photocatalyst concentrations and pH to study CBZ adsorption capacity. These measurements were performed at 25 °C and without any other factors present. Photolysis reaction was also studied at pH = 7 and pH = 5, T = 25 °C, with flux intensity of 60 $mW\cdot cm^{-2}$ and without introducing any other factors.

Table 1
Investigated factors and their levels.

Factor	Coded levels and their values				
	-a	-1	0	1	a
photocatalyst loading ($g\cdot dm^{-3}$)	0.25	0.5	1	1.5	2
temperature (°C)	10	20	25	30	40
flux ($mW\cdot cm^{-2}$)	30	35	45	60	70
pH	3	5	7	9	11
aeration ($dm^3\cdot h^{-1}$)	0	0	3	4	7
H_2O_2 addition (mM)	0	0	0.687	1.375	1.875

Following the optimization procedure, additional degradation runs presented in the discussion part were performed with 0.5 $g \cdot dm^{-3}$ of the photocatalyst loading, 60 $mW \cdot cm^{-2}$ of flux intensity, at 25 °C and without additional aeration. The solution pH and H_2O_2 presence were varied during these measurements and are defined along with the discussion. Additional experiments with pure TiO_2 particles and without photocatalyst were performed in analogous conditions.

Outside of CBZ removal, other responses were min-max normalized (details in Supporting Materials) to provide better clarity throughout the study and are presented in such values if not stated otherwise.

2.3. Analytical procedures

The CBZ degradation was monitored using a high-performance liquid chromatography system (HPLC), equipped with a C18 column with bound residual silane groups (Phenomenex, USA, model 00 F-4435-E0) and DAD photodiode array detector (Shimadzu, Japan, model SPD-M20A). During measurement, the temperature was kept at 45 °C, and isocratic flow of 1.5 $cm^3 \cdot min^{-1}$ was used with a mobile phase consisting of 68% H_2O, 31.6% acetonitrile, and 0.4% H_3PO_4 (85% solution) by volume. All reagents used as a mobile phase were HPLC-grade. Acetonitrile and phosphoric acid were provided by Merck (Germany) and VWR (Poland), respectively. Before experimentation, calibration was performed using dilution series of CBZ solution and its commercially available by-products: acridine (AC), acridone, acridine-9-carbaldehyde, 10,11-epoxy-carbamazepine (EP-CBZ), oxcarbazepine, and 10,11-dihydro-10,11-dihydroxy-carbamazepine. Pure (≥ 97%) compounds were provided by Sigma-Aldrich.

Besides chromatographic measurements, total organic carbon (TOC) analysis was performed using TOC-L equipment (Shimadzu, Japan).

For each irradiation cycle, a total number of five HPLC samples were collected at 0, 30, 60, 90, and 120 min of irradiation together with additional samples collected at 60 and 120 min for TOC analysis.

Additional analysis was performed for selected samples using liquid chromatography- quadrupole time of flight mass spectrometry (LC-TOFMS) system to identify possible by-products of CBZ degradation, which have not fitted to signals of obtained pure compounds. Measurements were performed using LC system 1200 Infinity (Agilent, USA) series consisting of the thermostated autosampler, binary pump, thermostated column compartment, additional DAD (diode array detector), and QTOF 6540 (Agilent, USA). All modules were controlled by MassHunter v B9.0 and B7.0, and this software was used for data collection and processing. The final optimized method for separating possible by-products utilized the Zorbax XDB-C8 column (150 × 4.6 mm, 3 μm). The chromatographic conditions were as follows: flow rate 0.8 $cm^3 \cdot min^{-1}$ in isocratic mode consisting of 60% H_2O and 40% of acetonitrile v/v, the temperature of separation was kept at 35 °C, while injection volume was $5 \cdot 10^{-3}$ cm^3 in each analysis. The parameters of detection and ionization were as follows: data gathering in SCAN mode of MS in the range 50–300 *m/z* gas temperature 300 °C, drying gas flow 8 $dm^3 \cdot min^{-1}$, nebulizer gas flow 35 psig, the voltage of capillary, fragmentor, and skimmer were kept at 3500, 60 and 60 V respectively.

3. Results

3.1. Characterization of Fe_3O_4@SiO_2/d-TiO_2/Pt magnetic photocatalyst

The XRD pattern has shown signals originating from the anatase, rutile, and magnetite Fe_3O_4 phases (see Fig. 1). The nanoparticles exhibit the intense peak at $2\theta = 35.2°$ corresponds to the (311) reflection of Fe3O4 cubic spinel structure according to the standard XRD spectrum (JCPDS card No. 89–3854). The broad diffraction peak at $2\theta = 15–20°$ is related to an amorphous silica layer in the nanocomposite structure. The diffraction peaks of TiO_2 can be attributed to (101), (103), (200), and (105) reflections of anatase (JCPDS card No. 89-4203), and (110), (101), (200) reflections of rutile (JCPDS, No. 76–1940). The most intense diffraction peaks of magnetite (Fe_3O_4) in the XRD patterns at 35.2° became significantly weaker due to the formation of the SiO_2-d-TiO_2 shell on the surface of ferrite particles. Moreover, the XRD analysis did not show any additional peaks from impurities, e.g., Fe_2TiO_5 phase, confirming effective coverage of magnetite by SiO_2. The direct contact between Fe_3O_4 and TiO_2 during the calcination process would result in the migration of Fe^{3+} ions to TiO_2 and formation of pseudobrookite (Fe_2TiO_5), and further photo-dissolution of Fe may take place during photodegradation, thus affecting the whole process.

The results are consistent between all synthesized batches, suggesting good repeatability of the preparation procedure. The detailed mean phase composition and crystallites size obtained from the XRD analysis is presented in Table 2, together with the calculated relative standard deviation between the batches. The surface area of the obtained composite was about 117 $m^2 \cdot g^{-1}$ and relatively constant for different batches.

The formation of the final composite structure was confirmed with HRTEM analysis, with the exemplary images shown in Fig. 2. Moreover, as shown in Fig. S1, performed mapping confirms surface localization of the TiO_2 shell, compared to SiO_2 interlayer and the oxygen-rich core of

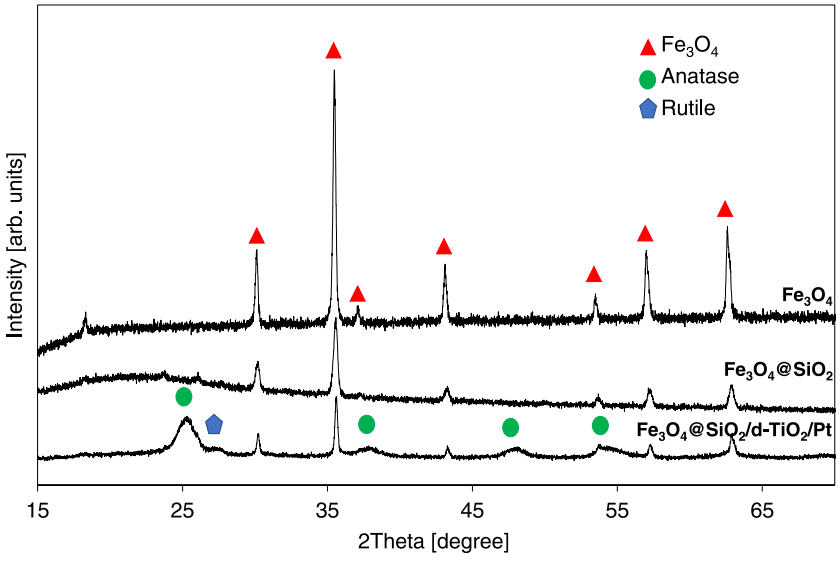

Fig. 1. Typical XRD diffraction pattern of the obtained nanocomposite.

Table 2
Characterization of the Fe_3O_4@SiO_2/d-TiO_2/Pt magnetic photocatalyst.

Value	BET surface area [$m^2 \cdot g^{-1}$]	Anatase [%] (size [nm])	Rutile [%] (size [nm])	Magnetite [%] (size [nm])
Mean	117	69 (5.5)	8 (9.0)	23 (43.0)
RSD [%]	4	3.6 (1.0)	5.0 (1.4)	11.1 (5.5)

Fe_3O_4.

The bandgap of the obtained TiO_2 shell was found to be 3.25 eV, as determined using the Tauc method, which originates from the direct electron transfer between valence and conduction bands of anatase. For higher wavelengths, an increase of absorbance resulted from the absorption of the Fe_3O_4 core and minority rutile phase as well as defect states introduced with V_{Ti} [22]. Moreover, Pt nanoparticles' presence was confirmed as the intense maximum peak at 410 nm [24], when Fe_3O_4@SiO_2/d-TiO_2 without platinum was used as a reference (see in Fig. 3c). The electron paramagnetic resonance (EPR) analysis confirmed the presence of titanium vacancies with *g* value of 1.995.

To study the Fe_3O_4@SiO_2/d-TiO_2/Pt photocatalysts' surface properties, the electrophoretic mobility of Fe_3O_4, SiO_2, d-TiO_2/Pt, and Fe_3O_4@SiO_2/d-TiO_2/Pt particles at different pH values was investigated. The isoelectric point (IEP), which represents the pH where the electrophoretic mobility changes from positive to negative, for Fe_3O_4@SiO_2/d-TiO_2/Pt was estimated at pH of 4 (see Fig. 4).

For Fe_3O_4@SiO_2/d-TiO_2/Pt photocatalyst, the surface was positively charged below pH of 4 and negatively charged above the IEP value. The isoelectric point for d-TiO_2/Pt is significantly different from the IEP for commercial TiO_2 P25, suggesting that modification of TiO_2 crystal structure and deposition of Pt NPs alters the charge distribution over the surface of the obtained composite core-shell photocatalyst [25,26]. According to the literature, the surface charge of the Pt modified photocatalyst is more positive than the pure semiconductor leading to different adsorption behavior [27]. The surface charge of Fe_3O_4@SiO_2/d-TiO_2/Pt is related to the outermost surface charge photoactive layer of d-TiO_2/Pt, which is responsible for the interaction between the composite and carbamazepine.

3.2. Optimization – Estimation of experimental error

The estimation of possible variation was based on the standard deviation (*s* value) between repeated measurements at the central point of the design (all factors at "0" level). The results of CBZ and TOC removal are presented in Table 3, together with the formation of selected by-products. Obtained *s* values were mainly within the range of ± 2%, with the highest variance observed for the normalized formation of hydroxy-carbamazepine (OH-CBZ) with the value of $s = 6\%$.

3.3. Dark reaction and photolysis

The results of the dark reaction series are shown in Fig. 5. Minimal adsorption of CBZ occurred in the presence of Fe_3O_4@SiO_2/d-TiO_2/Pt photocatalyst (up to 3%), and almost no dependence on pH was observed. This is consistent with the analysis of the zeta potential of Fe_3O_4@SiO_2/d-TiO_2/Pt photocatalyst in a function of pH. Since the pKa value for carbamazepine is about 13.9, it is expected that carbamazepine degradation is pH-independent, and CBZ will be primarily present in its protonated form ($CBZH^+$).

These results are in agreement with the literature since TiO_2 is known to efficiently adsorb many pollutants, mostly under light

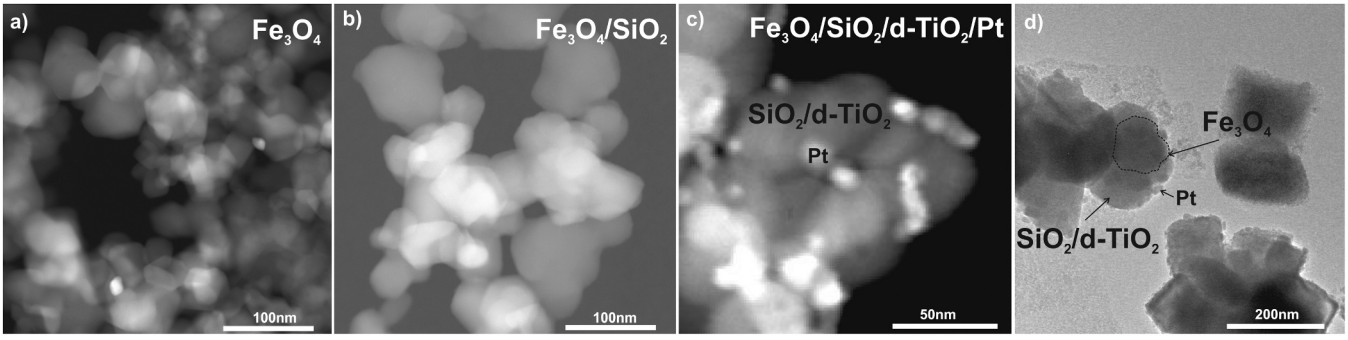

Fig. 2. TEM images presenting all stages of building the core-shell defective Fe_3O_4@SiO_2/d-TiO_2/Pt magnetic nanocomposite: Fe_3O_4 (a), Fe_3O_4@SiO_2 (b), and final composite (c-d).

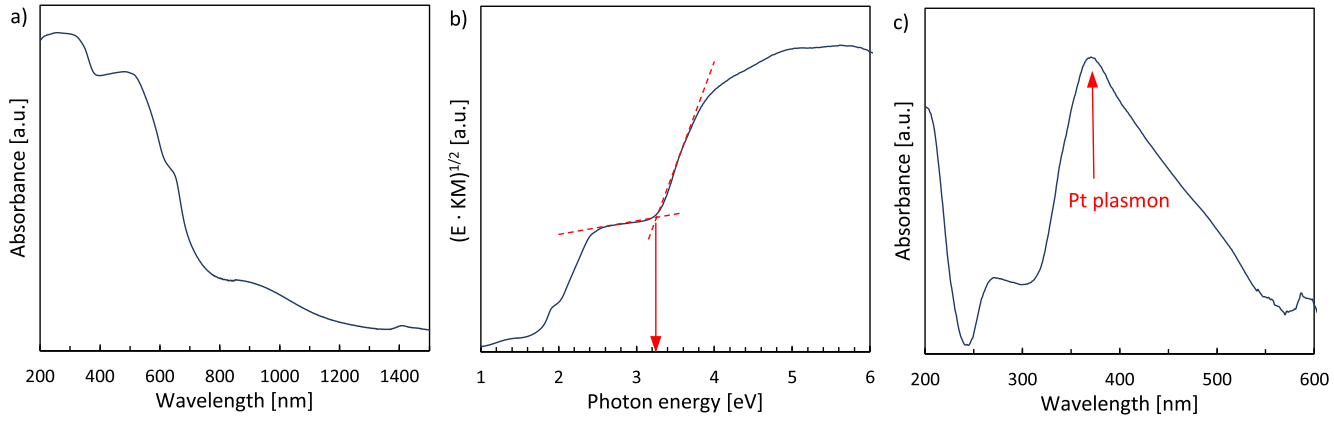

Fig. 3. DR-UV/Vis spectrum of the obtained nanocomposite (a) together with its transformation and bandgap determination using Tauc method (b) and observed Pt plasmon (c).

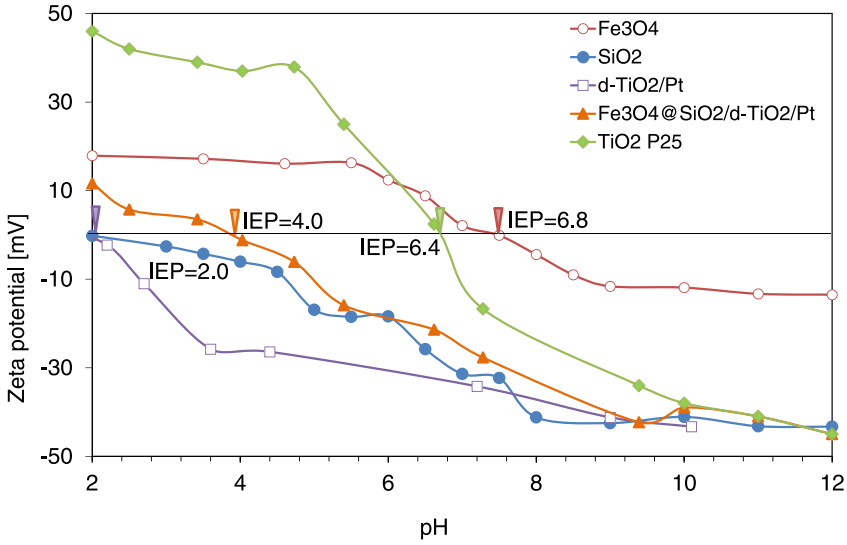

Fig. 4. Zeta potential as a function of pH for Fe_3O_4@SiO_2/d-TiO_2/Pt composite as well as Fe_3O_4, SiO_2, d-TiO_2/Pt, and commercial TiO_2 P25 nanoparticles.

Table 3
Estimation of experimental error as a standard deviation of selected responses.

Measurement	CBZ degradation	TOC removal	Acridine formation	OH-CBZ formation
1	0.550	0.581	0.092	0.970
2	0.514	0.621	0.066	0.851
3	0.517	0.590	0.056	0.930
s	**0.020**	**0.021**	**0.019**	**0.061**

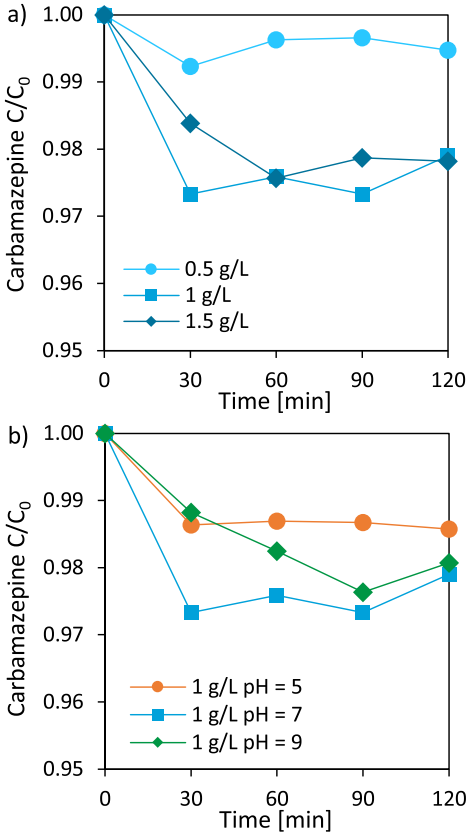

Fig. 5. CBZ adsorption capacity during dark reaction for different photocatalyst concentrations (a) and pH (b).

irradiation [28]. For the photolysis process, the observed CBZ removal was about 7% at pH = 7% and 30% at pH = 5.

3.4. CBZ removal and mineralization

The overall results showed that CBZ degradation efficiency ranging from 38% to 96%, and analysis of the obtained data was started by fitting regression model including 2-factor interactions and quadratic terms, according to general Eq. (1):

$$y = \beta_0 + \sum_{i=1}^{n} \beta_i x_i + \sum_{i=1}^{n} \beta_{ii} x_i^2 + \sum_{i=1}^{n} \sum_{j=i+1}^{n} \beta_{ij} x_i x_j \quad (1)$$

where y is a response, β_0 is constant, n is a number of individual factors, β are coefficients (specific for each term in full equation), and x are subsequent factors.

Similar models were applied to all considered responses. The significance of analyzed terms was evaluated using analysis of variance (ANOVA) calculations. Model calculations were performed using Minitab 2019 software at a 5% significance level ($\alpha = 0.05$). The obtained results of overall CBZ degradation efficiency are presented in Fig. 6. The significant effect of pH is visible, which was further proven by ANOVA calculations.

Fig. 7a shows the significance of terms included in the regression model for CBZ removal, revealing a combination of pH and H_2O_2 addition as the main factors responsible for enhancing the degradation process. It can be seen in Fig. 7b that interactions between these two factors have led to approximately doubling the reaction efficiency when H_2O_2 is added in acidic pH. The effect of temperature and flux intensity increase also promoted CBZ removal, while the relatively small impact of photocatalyst loading and aeration was observed.

On the other hand, as presented in Fig. 8a, photocatalyst loading and aeration, including their interactions, significantly affected the mineralization process. It could also be noted that, despite the general similarity, the correlation between CBZ and TOC removal as a function of pH was not observed in the neutral conditions, as presented in Fig. 8b.

Since it was expected that pH affects TiO_2 reactivity and its interactions with the organic species [29,30], further analysis was performed inside different pH regions. The summary of the obtained models is presented in Table 4. The terms included higher in the table are more significant, and the sign next to them indicates their effect on the response when shifted toward higher levels: (+) means a positive, (-) a negative impact on CBZ and TOC removal. Additional terms are considered as "possible" to affect the process if their calculated effect was

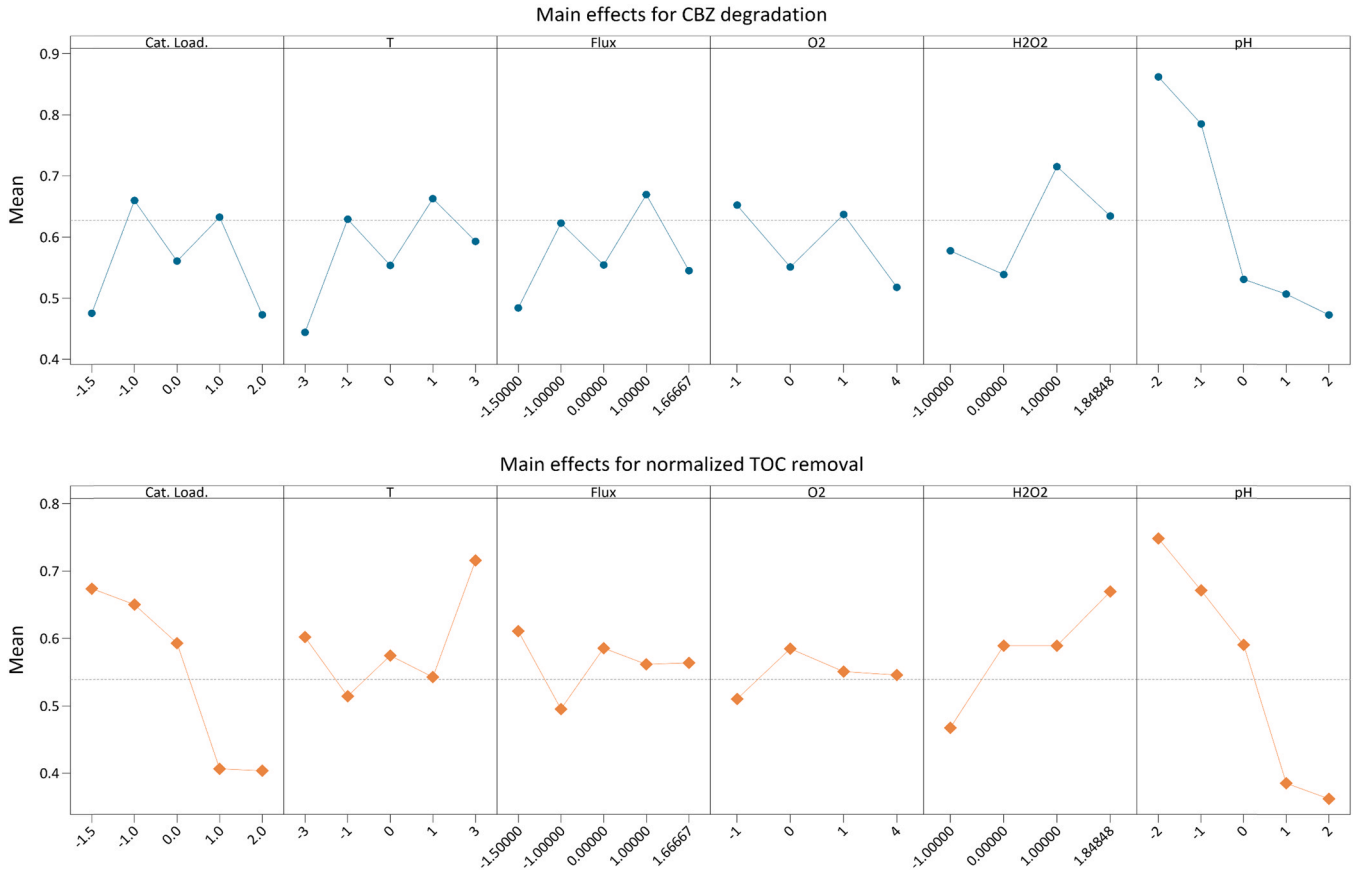

Fig. 6. Obtained effects of main factors on CBZ degradation (up) and TOC removal (down). The Grey line indicates a global mean.

close to the critical value (within the error). When comparing the obtained results, it is visible that pH changes the character of the ongoing process. Decreasing pH from 7 resulted in more factors affecting both CBZ and mineralization. Also, H_2O_2 addition became more significant than in neutral or basic conditions. It is also noticeable that flux intensity or its interactions became more significant in the alkaline conditions, while they are not present or relatively less important in pH $\leq$ 7.

3.5. *By-products formation*

The intermediate compounds identified during the photodegradation process are listed in Table 5. The most commonly found by-products include hydroxy-carbamazepine (OH-CBZ) and acridine (AC), which were present in most of the analyzed samples. Additionally, an acridone (ACD) presence was found in samples obtained in alkaline conditions. The observed degradation by-products are in agreement with the literature [31,32]; however, some differences are still present. Mainly, the hydroxy-carbamazepine (OH-CBZ) and 10,11-epoxy-carbamazepine (EP-CBZ), both reported as possible by-products, have $m/z = 253$ and were found to co-eluting in the adapted conditions. In this regard, their formation was analyzed based on both DAD and TOFMS analyses. Fig. 9a presents the sample's absorption spectra (ascribed to OH-CBZ) together with pure EP-CBZ and a solution, where epoxide was added as an internal standard to the sample. It was found that epoxide presence shifts the main signal to 209 nm and suppresses the second one at 297 nm. Since no defined maximum at 209 nm was noticed in the real sample, and 212 nm peak was always present together with 297 nm, the $m/z = 253$ signal was ascribed to the predominant formation of OH-CBZ. Analyzed spectrum also shows visible similarities to pure carbamazepine, with the main difference being 285 nm maximum red-shifted to 297 nm, as shown in Fig. 9b. This could be due to the -OH group being an electron-donor group and causing adsorption red-shift through a mesomeric effect when a simple substitution occurs in a CBZ conjugated system [33].

From the identified compounds, acridine and hydroxy-carbamazepine could be seen as the most interesting ones. AC formation is known to be a result of carbamazepine photolysis, while at the same time, hydroxylation is often the first step of photocatalytic oxidation. In this regard, both were selected as additional factors, possibly indicating differences in the performed process of photolysis and photocatalysis. Performed analysis and fitted model was the same as in the case of CBZ removal, and both OH-CBZ and AC signals were min-max normalized throughout the results. Normalized acridine concentration ranged from no presence to approximately 290 $\mu g \cdot dm^{-3}$, based on performed calibration, while the formation of hydroxy-carbamazepine was monitored as a peak area for a signal detected at 297 nm. The obtained results, with the most significant terms, are presented in Table 6.

Overall analysis suggests the presence of a strong, pH-dependent maximum/minimum due to the high significance of the pH^2 terms. Indeed, these optima are visible, as presented in Fig. 10 shows enhancement of OH-CBZ formation at neutral conditions and acridine suppression for pH = 7 and pH = 5.

A strong dependence of by-products' quality on process pH correlates well with observed differences in CBZ removal. Therefore, a detailed analysis of their concentration during the process was studied concerning pH, H_2O_2 presence, and removal of CBZ itself. As presented in Fig. 11a, it was noticed that acridine formation in alkaline pH was connected with a constant increase of its concentration over CBZ degradation time, suggesting that further oxidation of AC might be the limiting step of the whole process. Furthermore, increasing acridine content resulted in acridone formation, which was detected only for samples obtained at alkaline conditions. Other observations could be made by analyzing differences between AC formation in neutral and

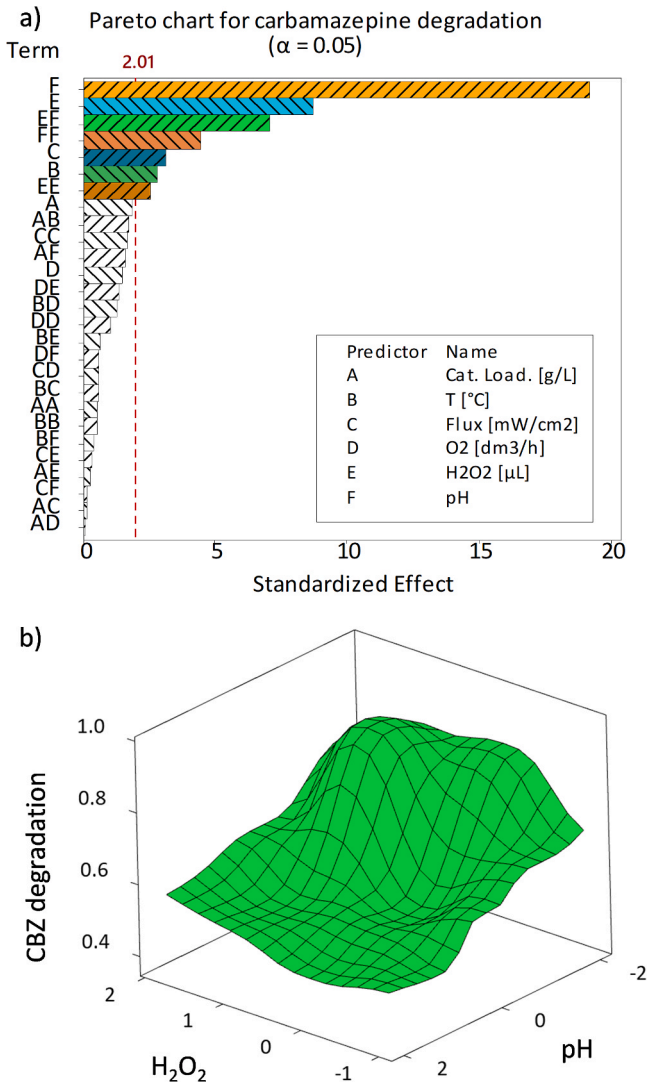

Fig. 7. Calculated effect of included terms on carbamazepine removal (a) and 3D representation of pH and H_2O_2 interaction (b).

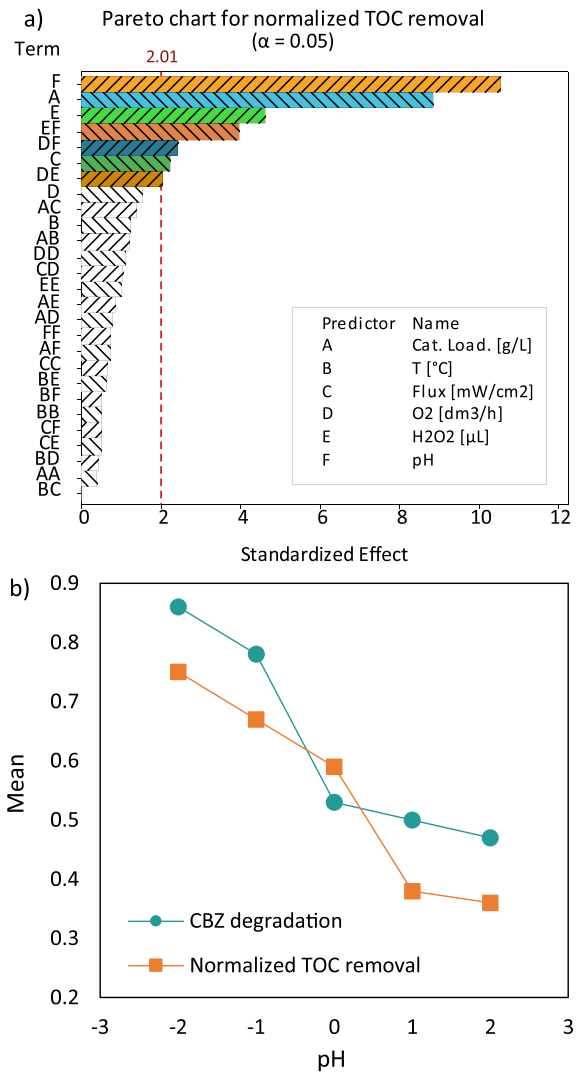

Fig. 8. Calculated effect of included terms on TOC mineralization (a) and the pH effect on CBZ and TOC removal (b).

acidic conditions. Decreasing pH from 7 to 5 slightly increase acridine presence was noticed. However, H_2O_2 addition at the strongly acidic conditions (pH = 3) seems to be limiting the acridine concentration and strongly enhancing carbamazepine removal, as shown in Figs. 11a and c.

An opposite situation was observed for OH-CBZ, which formation was suppressed at pH > 7, while a constant increase was observed mainly in neutral conditions (Fig. 11b). In this case, a further decrease of pH slightly promoted the initial formation of OH-CBZ, which later undergo a moderate increase or starts to drop, depending on the presence of H_2O_2. Since hydroxy-carbamazepine is the first possible product of CBZ oxidation and acts as a substrate for further oxidation, these results illustrate intensification of the process and subsequent OH-CBZ oxidation for the H^+/H_2O_2-assisted process.

4. Post-optimization discussion

4.1. Comparison with pure TiO_2

Performed optimization shows that a combination of H^+ and H_2O_2 addition is crucial to achieve high CBZ removal and mineralization. However, primarily suppression of the process efficiency in alkaline conditions is opposite to the results presented by Im et al., who have found that an increase of pH can enhance CBZ removal when using pure TiO_2 photocatalyst [34]. Therefore, additional CBZ degradation tests were performed using pure TiO_2 nanoparticles prepared from titanium tert-butoxide (TBT) as a reference. As shown in Fig. 12, the obtained results showed that synthesized TiO_2 and Fe_3O_4@SiO_2/d-TiO_2/Pt magnetic nanocomposite react differently to the change of process environment.

It is especially noticeable that pure TiO_2 exhibited the highest efficiency under alkaline conditions, while the obtained magnetic composite revealed higher activity only at acidic conditions and with H_2O_2 addition (see Fig. 12). This change is remarkable and should directly result from the differences in the photocatalyst structure. For the pure TiO_2, the enhancement of the CBZ degradation under alkaline conditions was connected with the positively charged CBZ molecule's preferred adsorption on the negatively charged, photo-excited surface of TiO_2 [35]. Then, the adsorbed molecule reacts with generated radicals, mainly due to the possible involvement of ^-OH ions, as shown in Eq. (2) [36]:

$$h^+ + \overline{O}H \rightarrow \cdot OH \quad (2)$$

These results are in agreement with the control TiO_2 sample analysis. However, the magnetic composite behaves differently. Since the CBZ nature does not change between measured series and EDX/EIP analysis confirmed the surface presence of negatively charged TiO_2 shell, the

Table 4
Comparison of terms' significance obtained in different pH regions for CBZ and TOC removal. Terms included higher are more significant.

Response	Effect	Whole pH range	pH < 7	pH = 7	pH > 7
CBZ removal	Significant	pH (-) H_2O_2 (+) pH·H_2O_2 (-) pH^2 (+) Flux (+) Temp. (+) $H_2O_2^2$ (+)	H_2O_2 (+) Cat.load (-) Flux (+) Temp (+) Flux·O_2 (-) Cat.load·Temp (+)	Temp (+) $H_2O_2^2$ (+)	Flux (+) O_2·H_2O_2 (+)
	Possible	Cat.load (-) Cat.load·Temp (+)	Cat.load·O_2 (-)	–	Temp·O_2 (-)
TOC removal	Significant	pH (-) Cat.load (-) H_2O_2 (+) pH·H_2O_2 (-) O_2·pH (-) Flux (+) O_2·H_2O_2 (-)	H_2O_2 (+) Cat.load (-) O_2 (+) O_2·H_2O_2 (-)	Cat.load (-) H_2O_2 (+)	Cat.load (-) Cat.load·Temp (+) Flux·H_2O_2 (-)
	Possible	–	Temp·H_2O_2 (+) Flux (+)	Temp. (+)	–

Table 5
Information about identified by-products.

Identified compound		Chemical structure	Characteristics
DAD and TOFMS	Carbamazepine	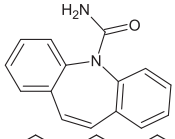	λ_{max} = 212 nm; 285 nm m/z = 237
	Acridine	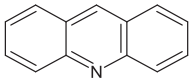	λ_{max} = 255 nm m/z = 180
	Acridone	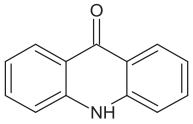	λ_{max} = 255 nm m/z = 196
	Hydroxy-carbamazepine	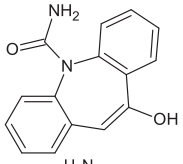	λ_{max} = 212 nm; 297 nm m/z = 253
TOFMS	10,11-dihydro-dihydroxy-carbamazepine	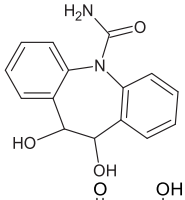	m/z = 271
	Acridone-hydroxide	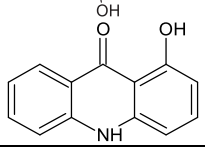	m/z = 226

possible photo-adsorption should be similar. Therefore, it was concluded that reaction (2) could not occur for the Fe_3O_4@SiO_2/d-TiO_2/Pt photocatalyst. Decreased ability of the composite to produce reactive radicals under high pH would also explain the observed increase of acridine and acridone concentrations, as photolysis by-products [36,37] as well as the relative absence of OH-CBZ. Further, this explains the significance of flux intensity on CBZ removal in alkaline conditions, while other factors were relatively less important.

The presented differences are further reflected in the interactions between H^+ and H_2O_2 in the photocatalyst presence. Reactivity of coupled H_2O_2/TiO_2 systems was already reported [38,39], and it enhances the decomposition of organic pollutants. However, some maximum is usually observed when increasing H_2O_2 concentration due to the variety of possible reactions. In this study, the initial optimization boundaries do not show maximum efficiency for a high H_2O_2 amount. Moreover, the superior performance of Fe_3O_4@SiO_2/d-TiO_2/Pt presented in Fig. 12 was shown only for a specific H_2O_2 addition. Therefore, the effect of H_2O_2 concentration for pure TiO_2 and Fe_3O_4@SiO_2/d-TiO_2/Pt samples was further studied in detail. Fig. 13 presents the obtained results of CBZ degradation for the control TiO_2 sample, Fe_3O_4@SiO_2/d-TiO_2/Pt, and simple photolysis at the pH of 5.

The obtained results showed that pure TiO_2 exhibited high enhancement of degradation efficiency for a lower H_2O_2 concentration, while it started to follow the efficiency of simple photolysis from C_{H2O2}

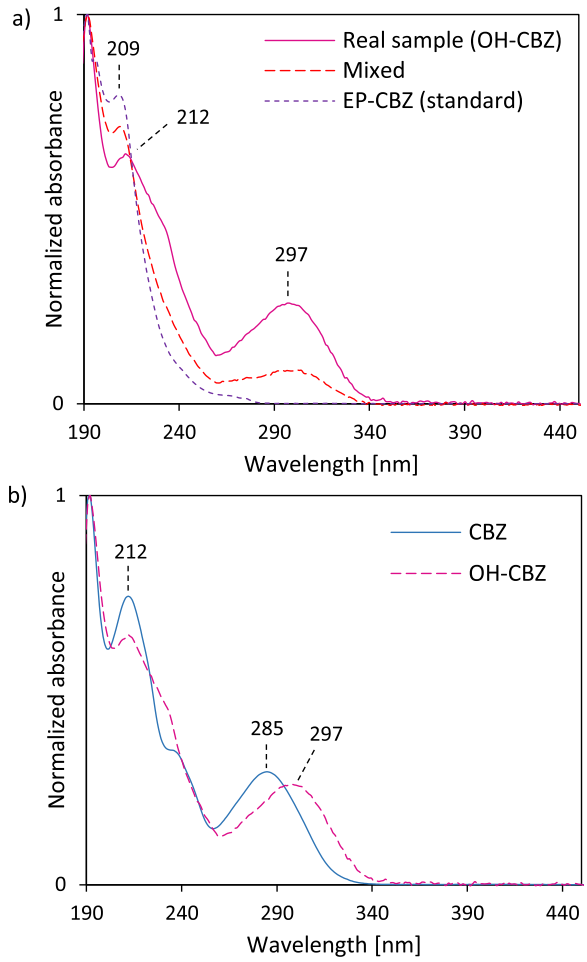

Fig. 9. The obtained absorbance spectra for hydroxy-carbamazepine, epoxy-carbamazepine and their mixture (a) and comparison between spectra of carbamazepine and hydroxy-carbamazepine (b).

= 1.375 mM. It is remarkable that at this point, the concentration of hydrogen peroxide already exceeded CBZ concentration approximately 23 times. In this regard, it is especially possible for the photogenerated charge carriers to start reacting with both H_2O_2 and the previously generated reactive oxygen species (ROS) instead of simply initiating the degradation process. Possible reactions, including both h^+ and e^- presence, are given by Eqs. (3–6), for which especially (4) and (5) are the reverse of (3) and (6) [34].

$$H_2O_2 + e^- + H^+ \rightarrow \cdot OH + H_2O \quad (3)$$

$$\cdot OH + H_2O + h^+ \rightarrow H_2O_2 + H^+ \quad (4)$$

$$H_2O_2 + h^+ \rightarrow \cdot HO_2 + H^+ \quad (5)$$

$$H^+ + \cdot HO_2 + e^- \rightarrow H_2O_2 \quad (6)$$

The increased rate of the consecutive reactions between charge carriers and different ROS is mainly recognized as the limiting factor for the TiO_2/H_2O_2 systems under the high H_2O_2 concentration. In this case, the monotonous increase of the degradation efficiency for $Fe_3O_4@SiO_2$/d-TiO_2/Pt nanocomposite especially suggests that generated species do not undergo further reactions with charge carriers. When confronted with the results presented in Fig. 12, it was noticed that the reactivity of photogenerated h^+ must be limited for the discussed composite. Therefore, reaction (3) starts to be predominant for the investigated system, while reverse reaction (4) is hindered. This reasoning directly connects $\cdot OH$ generation with both H_2O_2 presence and H^+ concentration, which agrees with a similar efficiency of CBZ removal obtained for the pH = 5 with 1.375 mM H_2O_2 process and pH = 3 and 0.687 mM H_2O_2 (a double peak in Fig. 7b).

These results could be explained based on the photocatalyst structure and possible charge carriers separation. It is known that Pt presence should increase the reactivity of photogenerated e^- through its transfer

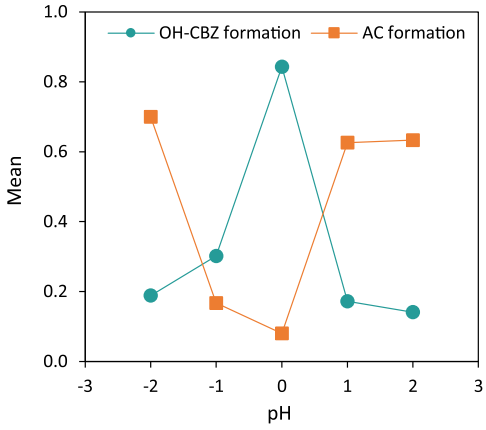

Fig. 10. Dependence of hydroxy-carbamazepine (OH-CBZ) and acridine (AC) formation on process pH.

Table 6
Comparison of terms' significance obtained in different pH regions for OH-CBZ and acridine formation. Terms included higher are more significant.

Response	Effect	Whole pH range	pH < 7	pH = 7	pH > 7
OH-CBZ formation	Significant	pH^2 (-) Cat.load^2 (-) $H_2O_2^2$ (-) Cat.load. (+) Flux^2 (-) pH·H_2O_2 (+) pH (-) H_2O_2 (-) Temp^2 (-) Temp (+)	H_2O_2 (-) Cat.load. (+) Temp (+) Temp·H_2O_2 (-) Flux·Temp (-)	–	Cat. Load (+) Flux (-) O_2 (-) T·O_2 (-) Cat.load·Temp (+) H_2O_2 (+) Temp·H_2O_2 (+)
	Possible	–	Flux·O_2 (+) Flux (-)	–	Flux·O_2 (+)
Acridine formation	Significant	pH (+) pH^2 (+) Temp·pH (+)	pH (-) Temp (-)	–	Temp (+)
	Possible	Temp·Flux (+) $H_2O_2^2$ (+) Flux^2 (+)	H_2O_2 (-)	–	Temp·Flux (+) Cat.load (+)

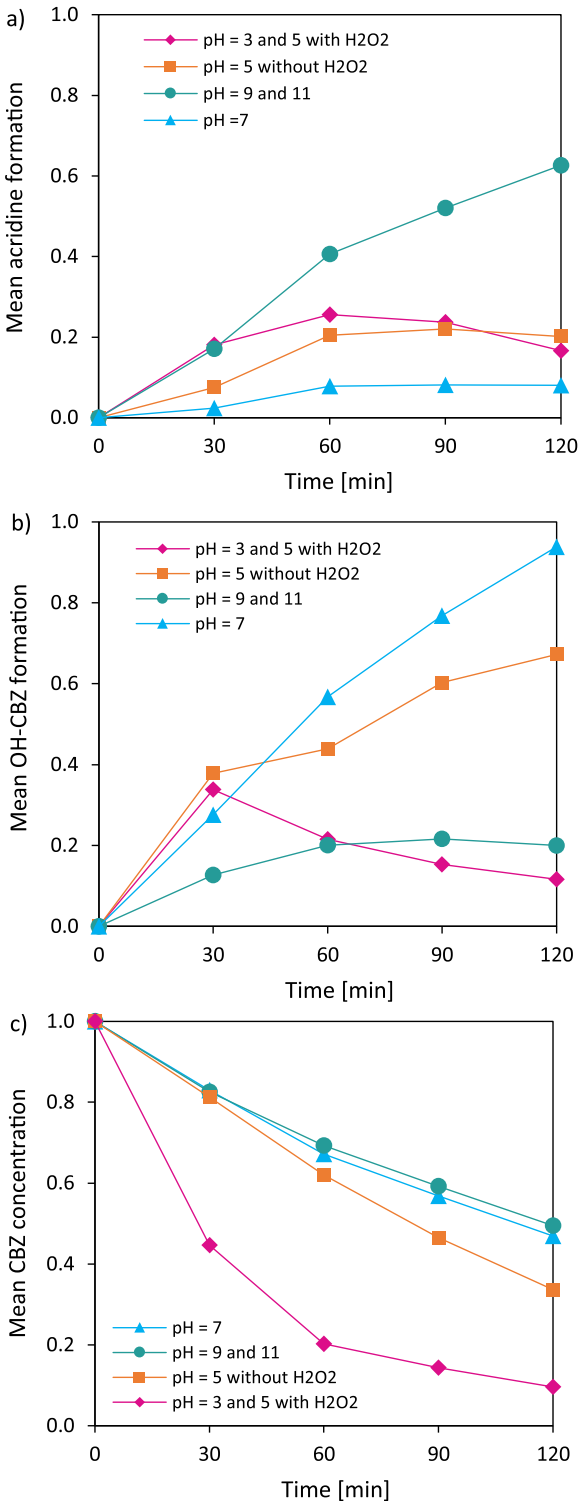

Fig. 11. Dependence of acridine (a) and hydroxy-carbamazepine (b) formation, together with carbamazepine removal efficiency (c) for different pH/H_2O_2 combinations.

from TiO_2 structure [19]. On the other hand, h^+ could be transferred to the Fe_3O_4 core; however, the presence of the SiO_2 layer inhibit such transition. Moreover, no formation of a secondary Ti-Fe phase (Fe_2TiO_5) was observed, e.g., during nanocomposite calcination, which further disproves a direct contact between TiO_2 and Fe_3O_4. Therefore, the effect of Ti^{4+} vacancies could be explained by trapping h^+ inside the photocatalyst shell [40]. As presented schematically in Fig. 14, this feature is

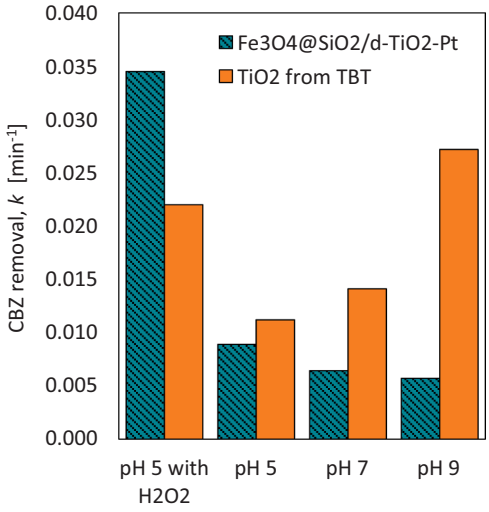

Fig. 12. Photocatalytic activity comparison between obtained Fe_3O_4@SiO_2/d-TiO_2/Pt nanocomposite and pure TiO_2 for different combinations of pH and H_2O_2 presence (1.375 mM). The preparation procedure for the control TiO_2 sample is given in SI.

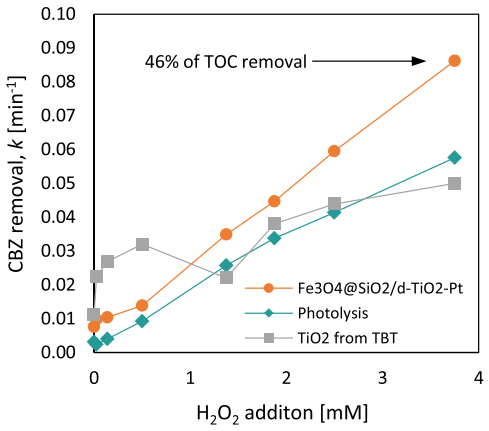

Fig. 13. Degradation efficiency comparison between control TiO_2, the obtained magnetic nanocomposite, and simple photolysis in the presence of different H_2O_2 concentrations.

primarily responsible for the observed differences and improved efficiency of the Fe_3O_4@SiO_2/d-TiO_2/Pt system in the presence of H_2O_2 relatively higher concentration. The magnetic composite's final CBZ degradation rate under simulated solar light (UV-Vis) was 2-times higher than the control TiO_2 sample. Moreover, the efficiency of carbamazepine removal in Vis light ($\lambda > 400$ nm) with the addition of H_2O_2 was about 57% after 120 min of irradiation (see Fig. S3 in ESI).

4.2. *Reusability of the Fe_3O_4@SiO_2/d-TiO_2/Pt photocatalyst*

The obtained nanocomposite was designed primarily to enable its easy separation after the process. Therefore, its performance was tested in eight subsequent degradation cycles, between which the photocatalyst was recycled in a magnetic field. The separated composite was used in the follow-up process without any pre-treatment. The process parameters were adapted as follows: 0.5 $g \cdot dm^{-3}$ photocatalyst dosage, 60 $mW \cdot cm^{-2}$ flux intensity, 25 °C, no aeration, pH = 5, and 1.375 mM H_2O_2 addition. The obtained results show the nanocomposite's excellent stability with no loss in the photocatalyst performance during all cycles. Fig. 15 shows the concentration curves for CBZ removal for all consecutive processes.

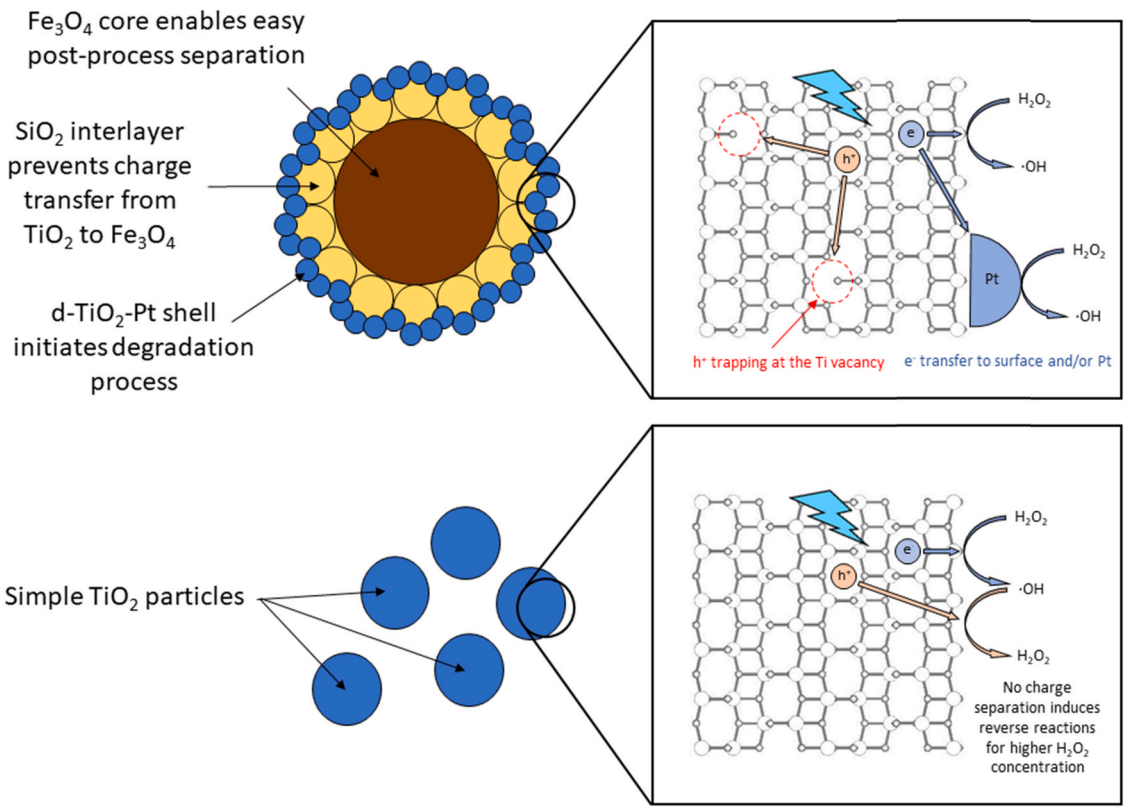

Fig. 14. Schematic representation of the photocatalyst structure and possible charge transfer mechanism for the obtained composite and control TiO_2 sample.

5. Conclusions

Magnetite particles were coated using silica interlayer and titanium-defected TiO_2 modified with Pt nanoparticles to obtain magnetically separable photocatalyst. The prepared composite was used to study carbamazepine (CBZ) removal in a wide range of possible process parameters. Furthermore, the obtained results were analyzed in detail concerning CBZ degradation, mineralization, and a selected by-products formation. For pure TiO_2, the highest efficiency of CBZ degradation was noticed at alkaline conditions. In contrast, for the obtained magnetic composite suppression of CBZ, degradation in alkaline conditions was observed, followed by increased acridine formation and a remarkable process enhancement in the presence of H_2O_2 and an acidic environment. It was found that the introduction of the Ti vacancies in the magnetic photocatalyst structure resulted in the hole trapping inside defective TiO_2, while Pt nanoparticles enhanced e^- separation, which contributed to the observed differences. Outside the pH and H_2O_2, other process parameters were less significant for both CBZ removal and mineralization, with lower photocatalyst dosage (minimum of 0.5 $g \cdot dm^{-3}$ was tested), higher flux intensity, and higher temperature, slightly promoting process efficiency. The optimized CBZ degradation rate for Fe_3O_4@SiO_2/d-TiO_2/Pt nanocomposite was 2-times higher than the control TiO_2 sample. Finally, the composite's stability was tested in 8 subsequent cycles of CBZ photocatalytic degradation, showing magnetic photocatalyst excellent stability and reusability.

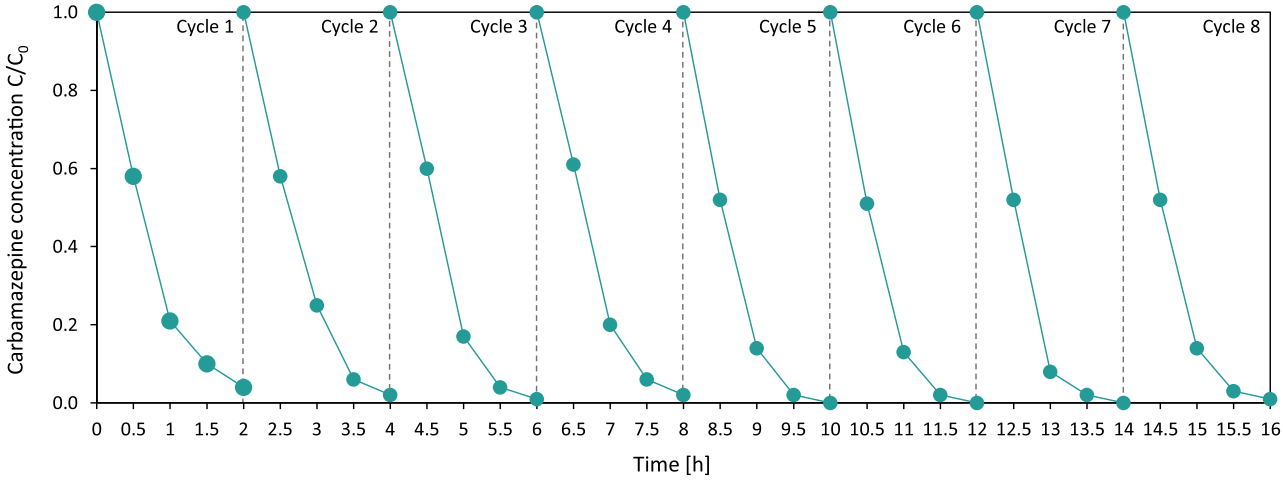

Fig. 15. Reusability of the Fe_3O_4@SiO_2/d-TiO_2/Pt nanocomposite for carbamazepine degradation under optimized conditions (pH = 5 with 1.375 mM of H_2O_2).

Funding

The research was financially supported by the Polish National Science Centre (grant no. 2016/23/D/ST5/01021 and NCN 2018/30/E/ST5/00845).

CRediT authorship contribution statement

Szymon Dudziak: characterization of the photocatalysts, HPLC analysis, optimization procedure, draft preparation, writing—review and editing. **Zuzanna Bielan:** investigation, synthesis of the photocatalysts, draft preparation, writing—review and editing. **Paweł Kubica:** HPLC-TOFMS analysis **Anna Zielińska-Jurek:** conceptualization, methodology, supervision, project administration, writing—review and editing, funding acquisition.

Declaration of Competing Interest

The authors declare that they have no known competing financial interests or personal relationships that could have appeared to influence the work reported in this paper.

Appendix A. Supporting information

Supplementary data associated with this article can be found in the online version at doi:10.1016/j.jece.2021.105782.

References

[1] S. Öllers, H.P. Singer, P. Fässler, S.R. Müller, Simultaneous quantification of neutral and acidic pharmaceuticals and pesticides at the low-ng/l level in surface and waste water, J. Chromatogr. A. 911 (2001) 225–234, https://doi.org/10.1016/S0021-9673(01)00514-3.

[2] T.A. Ternes, Occurrence of drugs in German sewage treatment plants and rivers1Dedicated to Professor Dr. Klaus Haberer on the occasion of his 70th birthday.1, Water Res. 32 (2002) 3245–3260, https://doi.org/10.1016/s0043-1354(98)00099-2.

[3] C.D. Metcalfe, X.-S. Miao, B.G. Koenig, J. Struger, Distribution of acidic and neutral drugs in surface waters near sewage treatment plants in the lower Great Lakes, Canada, Environ. Toxicol. Chem. 22 (2003) 2881–2889. http://www.ncbi.nlm.nih.gov/pubmed/14713027.

[4] R. Andreozzi, R. Marotta, N. Paxéus, Pharmaceuticals in STP effluents and their solar photodegradation in aquatic environment, Chemosphere 50 (2003) 1319–1330, https://doi.org/10.1016/S0045-6535(02)00769-5.

[5] E. Donner, T. Kosjek, S. Qualmann, K.O. Kusk, E. Heath, D.M. Revitt, A. Ledin, H. R. Andersen, Ecotoxicity of carbamazepine and its UV photolysis transformation products, Sci. Total Environ. 443 (2013) 870–876, https://doi.org/10.1016/j.scitotenv.2012.11.059.

[6] H. Chen, X. Gu, Q. Zeng, Z. Mao, Acute and chronic toxicity of carbamazepine on the release of chitobiase, molting, and reproduction in Daphnia similis, Int. J. Environ. Res. Public Health 16 (2019) 209, https://doi.org/10.3390/ijerph16020209.

[7] G. Vernouillet, P. Eullaffroy, A. Lajeunesse, C. Blaise, F. Gagné, P. Juneau, Toxic effects and bioaccumulation of carbamazepine evaluated by biomarkers measured in organisms of different trophic levels, Chemosphere 80 (2010) 1062–1068, https://doi.org/10.1016/j.chemosphere.2010.05.010.

[8] S. Wiegman, J.A.G. Termeer, T. Verheul, M.H.S. Kraak, P. de Voogt, R.W.P. M. Laane, W. Admiraal, U.V. Absorbance, U.V. absorbance dependent toxicity of acridine to the marine diatom Phaeodactylum tricornutum, Environ. Sci. Technol. 36 (2002) 908–913.

[9] S.R. de, O. Melo, M. Homem-De-Mello, D. Silveira, L.A. Simeoni, Advice on degradation products in pharmaceuticals: a toxicological evaluation, PDA J. Pharm. Sci. Technol. 68 (2014) 221–238, https://doi.org/10.5731/pdajpst.2014.00974.

[10] S. Bagheri, A. Termehyousefi, T. Do, Photocatalytic pathway toward degradation of environmental pharmaceutical pollutants: structure, kinetics and mechanism approach, Catal. Sci. Technol. 7 (2017) 4548–4569, https://doi.org/10.1039/C7CY00468K.

[11] S. Murgolo, I.S. Moreira, C. Piccirillo, P.M.L. Castro, G. Ventrella, C. Cocozza, G. Mascolo, Photocatalytic degradation of diclofenac by hydroxyapatite-TiO_2 composite material: Identification of transformation products and assessment of toxicity, Mater. (Basel) 11 (2018) 1–16, https://doi.org/10.3390/ma11091779.

[12] J.-R. Thelusmond, E. Kawka, T.J. Strathmann, A.M. Cupples, Diclofenac, carbamazepine and triclocarban biodegradation in agricultural soils and the microorganisms and metabolic pathways affected, Sci. Total Environ. 640–641 (2018) 1393–1410, https://doi.org/10.1016/j.scitotenv.2018.05.403.

[13] N.M. Nasir, S.A. Talib, S.N. Hashim, C.C. Tay, Biodegradation of carbamazepine using fungi and bacteria, J. Fundam. Appl. Sci. 9 (2017) 124–146.

[14] Y.F. Rao, L. Qu, H. Yang, W. Chu, Degradation of carbamazepine by Fe(II)-activated persulfate process, J. Hazard. Mater. 268 (2014) 23–32, https://doi.org/10.1016/j.jhazmat.2014.01.010.

[15] M. Soufan, M. Deborde, A. Delmont, B. Legube, Aqueous chlorination of carbamazepine: Kinetic study and transformation product identification, Water Res. 47 (2013) 5076–5087, https://doi.org/10.1016/j.watres.2013.05.047.

[16] S. Zhou, Y. Xia, T. Li, T. Yao, Z. Shi, S. Zhu, N. Gao, Degradation of carbamazepine by UV/chlorine advanced oxidation process and formation of disinfection by-products, Environ. Sci. Pollut. Res. 23 (2016) 16448–16455, https://doi.org/10.1007/s11356-016-6823-x.

[17] C. Byrne, G. Subramanian, S.C. Pillai, Recent advances in photocatalysis for environmental applications, J. Environ. Chem. Eng. 6 (2018) 3531–3555, https://doi.org/10.1016/j.jece.2017.07.080.

[18] H.-Y. Ma, L. Zhao, L.-H. Guo, H. Zhang, F.-J. Chen, W.-C. Yu, Roles of reactive oxygen species (ROS) in the photocatalytic degradation of pentachlorophenol and its main toxic intermediates by TiO_2/UV, J. Hazard. Mater. 369 (2019) 719–726, https://doi.org/10.1016/j.jhazmat.2019.02.080.

[19] I. Wysocka, E. Kowalska, K. Trzciński, M. Łapiński, G. Nowaczyk, A. Zielińska-Jurek, UV-Vis-induced degradation of phenol over magnetic photocatalysts modified with Pt, Pd, Cu and Au nanoparticles, Nanomater. (Basel, Switz.) 8 (2018), https://doi.org/10.3390/nano8010028.

[20] A. Zielińska-Jurek, Z. Bielan, S. Dudziak, I. Wolak, A. Zieli, Z. Sobczak, T. Klimczuk, G. Nowaczyk, J. Hupka, Design and application of magnetic photocatalysts for water treatment. The effect of particle charge on surface functionality, Catalysts 7 (2017) 360, https://doi.org/10.3390/catal7120360.

[21] M.R. Khan, T.W. Chuan, A. Yousuf, M.N.K. Chowdhury, C.K. Cheng, Schottky barrier and surface plasmonic resonance phenomena towards the photocatalytic reaction: study of their mechanisms to enhance photocatalytic activity, Catal. Sci. Technol. 5 (2015) 2522–2531, https://doi.org/10.1039/C4CY01545B.

[22] Z. Bielan, S. Dudziak, A. Sulowska, D. Pelczarski, J. Ryl, A. Zielińska-Jurek, Preparation and characterization of defective TiO_2. The effect of the reaction environment on titanium vacancies formation, Mater. (Basel) 13 (2020) 1–25, https://doi.org/10.3390/ma13122763.

[23] F. Zuo, K. Bozhilov, R.J. Dillon, L. Wang, P. Smith, X. Zhao, C. Bardeen, P. Feng, Active facets on titanium(III)-doped TiO_2: an effective strategy to improve the visible-light photocatalytic activity, Angew. Chem. 15 (2012) 6223–6226, https://doi.org/10.1002/anie.201202191.

[24] A. Zielińska-Jurek, Z. Wei, M. Janczarek, I. Wysocka, E. Kowalska, E. Size-controlled, Size-Controlled synthesis of Pt particles on TiO2 surface: physicochemical characteristic and photocatalytic activity, Catalysts 9 (2019) 940, https://doi.org/10.3390/catal9110940.

[25] M. Miyauchi, A. Ikezawa, H. Tobimatsu, H. Irie, K. Hashimoto, Zeta potential and photocatalytic activity of nitrogen doped TiO_2 thin films, Phys. Chem. Chem. Phys. 6 (2004) 865–870, https://doi.org/10.1039/b314692h.

[26] D.L. Liao, G.S. Wu, B.Q. Liao, Zeta potential of shape-controlled TiO_2 nanoparticles with surfactants, Colloids Surf. A Physicochem. Eng. Asp. 348 (2009) 270–275, https://doi.org/10.1016/j.colsurfa.2009.07.036.

[27] C. Hua, Y. Tang, Z. Jiang, Z. Hao, H. Tang, Po Keung Wong, Appl. Catal. A 253 (2003) 389–396.

[28] N. Sarmah, P.K. Bhattacharyya, K.K. Bania, Substituent and solvent effects on the absorption spectra of cation-π complexes of benzene and borazine: a theoretical study, J. Phys. Chem. A. 118 (2014) 3760–3774, https://doi.org/10.1021/jp5021966.

[29] A. Imanishi, T. Okamura, N. Ohashi, R. Nakamura, Mechanism of water photooxidation reaction at atomically flat TiO_2 (Rutile) (110) and (100) surfaces: dependence on solution pH, J. Am. Chem. Soc. 2 (2007) 11569–11578.

[30] A.P. Toor, A. Verma, C.K. Jotshi, P.K. Bajpai, V. Singh, photocatalytic degradation of direct Yellow 12 dye using UV/TiO_2 in a shallow pond slurry reactor, Dye. Pigment. 68 (2006) 53–60, https://doi.org/10.1016/j.dyepig.2004.12.009.

[31] Y. Pan, S.S. Cheng, X. Yang, J. Ren, J. Fang, C. Shang, W. Song, L. Lian, X. Zhang, UV/chlorine treatment of carbamazepine: Transformation products and their formation kinetics, Water Res 116 (2017) 254–265, https://doi.org/10.1016/j.watres.2017.03.033.

[32] X. Gao, W. Peng, G. Tang, Q. Guo, Y. Luo, Highly efficient and visible-light-driven BiOCl for photocatalytic degradation of carbamazepine, J. Alloy. Compd. 757 (2018) 455–465, https://doi.org/10.1016/j.jallcom.2018.05.081.

[33] N. Sarmah, P.K. Bhattacharyya, K.K. Bania, Substituent and solvent effects on the absorption spectra of cation-π complexes of benzene and borazine: a theoretical study, J. Phys. Chem. A. 118 (2014) 3760–3774, https://doi.org/10.1021/jp5021966.

[34] J.-K. Im, H.-S. Son, Y.-M. Kang, K.-D. Zoh, Carbamazepine degradation by photolysis and titanium dioxide photocatalysis, Water Environ. Res. 84 (2012) 554–561, https://doi.org/10.2175/106143012×13373550427273.

[35] N.M. Vieno, H. Härkki, T. Tuhkanen, L. Kronberg, Occurrence of pharmaceuticals in river water and their elimination in a pilot-scale drinking water treatment plant, Environ. Sci. Technol. 41 (2007) 5077–5084, https://doi.org/10.1021/es062720x.

[36] Y. Sun, J.J. Pignatello, Evidence for a surface dual hole-radical mechanism in the TiO_2 photocatalytic oxidation of 2,4-dichlorophenoxyacetic acid, Environ. Sci. Technol. 29 (1995) 2065–2072, https://doi.org/10.1021/es00008a028.

[37] S. Chiron, C. Minero, D. Vione, Photodegradation processes of the antiepileptic drug carbamazepine, relevant to estuarine waters, Environ. Sci. Technol. 40 (2006) 5977–5983, https://doi.org/10.1021/es060502y.

[38] K. Sahel, L. Elsellami, I. Mirali, F. Dappozze, M. Bouhent, C. Guillard, Hydrogen peroxide and photocatalysis, Appl. Catal. B Environ. 188 (2016) 106–112, https://doi.org/10.1016/j.apcatb.2015.12.044.
[39] M. Feilizadeh, F. Attar, N. Mahinpey, Hydrogen peroxide-assisted photocatalysis under solar light irradiation: Interpretation of interaction effects between an active photocatalyst and H_2O_2, Can. J. Chem. Eng. 97 (2019) 2009–2014, https://doi.org/10.1002/cjce.23455.
[40] B.J. Morgan, G.W. Watson, Polaronic trapping of electrons and holes by native defects in anatase TiO2, Phys. Rev. B - Condens. Matter Mater. Phys. 80 (2009) 2–5, https://doi.org/10.1103/PhysRevB.80.233102.